Precise Shape Engineering of Epitaxial Quantum Dots by Growth Kinetics

Sergio Bietti,[1] Juanita Bocquel,[2] Silvia Adorno,[1] Takaaki Mano,[3]
Joris G. Keizer,[2] Paul. M. Koenraad,[2] and Stefano Sanguinetti[1,*]

[1] *LNESS and Dipartimento di Scienza dei Materiali, Universitá degli Studi di Milano Bicocca, Milano, Italy*

[2] *Department of Applied Physics, Eindhoven University of Technology, The Netherlands*

[3] *National Institute for Materials Science, Tsukuba, Japan*

Abstract

We show that independent size and morphology engineering of epitaxial quantum dots can be obtained using a kinetically controlled quantum dot fabrication procedure, droplet epitaxy. Owing to the far-from-equilibrium droplet epitaxy procedure, based on the crystallization, under As flux, of a nanometric droplets of Ga, independent and precise tuning of quantum dot size, aspect ratio and faceting can be obtained. The dependence of the dot morphology on the growth conditions is interpreted and quantitatively described through a model taking into account the crystallization kinetics of the Ga stored in the droplet under As flux.

INTRODUCTION

Three dimensional semiconductor epitaxial nano-islands, or quantum dots (QDs), show a discrete spectrum of energy levels which make them the artificial equivalent of natural atoms [1]. Unlike and beyond natural atoms, QDs permits the fine tuning of their electronic properties by a precise engineering their morphology. Both their single-particle and many-particle characteristics depend in a non–trivial way on the QD size and shape [2, 3]. This reflects not only simple quantum-confinement physics, but also electronic structure effects such as interband, intervalley, spin-orbit, strain-induced state coupling [4, 5] and electron–phonon scattering probability [6–8]. The QD shape allows for the engineering of the QD electronic states in order to effectively extend the performance of various optoelectronic devices [9], ranging from room temperature QD-based inter-subband detectors [10] and lasers [11] to semiconductor optical amplifiers [12], polarization controlled single photon emitters for quantum communication systems [13, 14] and QD based photovoltaic cells [15–17]. In particular, by controlling QD size and aspect ratio (the ratio between QD height and diameter), it would be possible to tune independently QD emission energy and electron–phonon interaction, two relevant properties in QD based lasers, solar cells and detectors.

One of the most common methods for QDs fabrication is Molecular Beam Epitaxy (MBE) of lattice-mismatched III-V semiconductor materials via the Stranski-Krastanov (SK) mode [18]. SK exploits the self-assembly of pyramidal-like QDs driven by the relaxation of strain accumulated in the epilayer. Despite the high success of this technique which led to fundamental physical understandings of epitaxial QDs and to a large variety of applications [18–20], the available degree of freedom in remains limited [21] due to energetic driven evolution of the SK-QD shape [22]. A possible pathway to circumvent the limitations of SK-QD self–assembly is the use of a different paradigm for the fabrication of QDs. In this respect, the exploitation of a kinetics controlled epitaxial nano-island growth would overcome the limits imposed by the SK method which is characterized by nano-island shapes bound by an equilibrium set of facets that includes only stable surfaces [22].

Here we show that by using a kinetically driven epitaxial QD fabrication method, droplet epitaxy (DE) [23–26], a high degree of control over the QD size, aspect ratio and facet orientation angle (the angle between the substrate and the QD facet) is possible. GaAs/$Al_{0.3}GaAs_{0.7}$ DE-QDs, with volumes between from 10^2 to 10^5 nm^3, were obtained with a controlled as-

pect ratio ranging from 0.05 to 0.6 and a facet orientation angle from 10° to 55°. This was achieved by an accurate drive of the crystallization kinetics via growth parameters control. The morphology of the GaAs/AlGaAs DE-QDs was investigated by means of Atomic Force Microscopy (AFM) and cross-sectional Scanning Tunneling Microscopy (X-STM). We propose a model to interpret and quantitatively describe the mechanism governing the relationship between QD shape and the growth parameters based on Ga diffusion dynamics and crystallization during the exposure of the Ga liquid droplet to the As flux.

DE is an alternative growth procedure, based on Molecular Beam Epitaxy (MBE), for the self-assembly of epitaxial III-V semiconductor nanostructures which relies on growth kinetics to form three-dimensional nanostructures. The DE procedure is based on the subsequent deposition of III and V column elements at specific temperatures and fluxes. In short, DE growth of nanostructures in an MBE environment proceeds as follows. A III-column element molecular beam is initially supplied for the formation of droplets on the substrate surface in vacuum and subsequently an As flux is used for the crystallization of droplets into the III-As nanostructures. By a suitable selection of the growth conditions, carefully controlling the group III crystallization kinetics into III-V semiconductor, it is possible to engineer the final shape of the nanocrystals from islands [25, 27–29], rings [30, 31], wires [32, 33] and even more complex structures [34–39].

EXPERIMENTAL

DE-QDs were grown in a conventional MBE apparatus on GaAs (001) substrates. After the growth of a 100 nm $Al_{0.3}Ga_{0.7}As$ buffer layer, we performed DE, which consists of:

1. Ga droplet formation by a supply of Ga without As flux (background As pressure was below 1×10^{-9} Torr).

2. Crystallization of the Ga droplets into GaAs by a supply of As_4 flux with controlled pressures at various temepratures.

Droplets density and size are controlled during the Ga deposition step by the substrate temperature, the Ga flux and the total amount of Ga deposited. The As pressure and substrate temperature during the crystallization are used to control nanostructures morphology [30, 35, 37, 40]. Three sets of samples (P, T and V) were grown in this study. The detailed

growth parameters are summarized in Table I. For sets P and T, we prepared identical Ga droplets formed by a supply of 2.5 ML Ga at 350°C. In set P, droplets were crystallized at 200°C by a supply of different As beam equivalent pressure (BEP) ranging from 2.5×10^{-5} Torr to 5×10^{-6} Torr. In set T, the As BEP was fixed at 1×10^{-5} Torr while the droplets were crystallized at different substrate temperatures ranging from 150°C to 250°C. In set V, droplets of various size were crystallized under the identical conditions (supply of As (BEP 1×10^{-5} Torr) at 200°C). The droplet size was varied by controlling the total amount of deposited Ga (from 2 to 2.5 ML) and the substrate temperature during deposition (from 250°C to 350°C) The latter parameter, by acting on droplet density (from 1×10^{10} to 6×10^{8} cm^{-2} changes the amount of Ga stored in each single droplet. Within set V, we also grew a series of QDs with capping layer (V_{cap}) following the standard procedure for obtaining highly luminescent QDs, i.e. an uncapped annealing at 400°C and a post-growth rapid thermal annealing at 750°C [41]. In this subset, the Ga droplets were formed by a supply of 1.5 to 5 ML of Ga at 200°C and subsequently crystallized at 200°C by a supply of As flux of 2.5×10^{-4} Torr. This subset is of special importance as it allows us to investigate the QDs after capping in their functional state. We expect that complete crystallization of the Ga droplets into GaAs QDs occurs along with a wetting layer which a thickness less than a bilayer which originates from the change in surface reconstruction during the initial stages of Ga deposition[27, 42].

All samples were characterized by AFM in tapping mode using ultra-sharp tips with a 2 nm radius. In parallel, sample V_{cap} was investigated by X-STM performed at 77 K under UHV conditions (5×10^{-11} Torr). The STM was operated in constant current mode on clean and atomically flat (110) and ($1\bar{1}0$) GaAs surfaces obtained by *in-situ* cleavage. This scanning probe technique allows us to investigate at the atomic scale the morphology of the DE-QDs after capping.

RESULTS

For all sets of samples, a $c(4 \times 4)$ reconstruction was clearly visible in Reflection High Energy Electron Diffraction (RHEED) patterns before Ga deposition. The single ML of Ga required to subsequently onset the droplets formation as well as our experimental conditions [43] indicate that the $c(4\times4)\alpha$ phase is the most probable reconstruction at that initial stage.

TABLE I. Growth parameters of the different sets of samples. Set P: variation in As BEP. Set T: variation in crystallization temperature. Set V: variation in Ga droplet volume. Set V_{cap}: variation in Ga droplet volume and capping procedure.

Set	P	T	V	V_{cap}
Ga supplied (ML)	2.5	2.5	V1 = 3 V2 = 2 V3 = 2.5	C1 = 1.5 C2 = 2 C3 = 3 C4 = 5
Ga deposition T (°C)	350	350	V1 = 350 V2 = 350 V3 = 220	200
As BEP (10^{-6} Torr)	P1 = 50 P2 = 25 P3 = 10 P4 = 7.5 P5 = 5	10	10	250
Crystallization T (°C)	200	T1 = 150 T2 = 175 T3 = 200 T4 = 225 T5 = 250	200	200
Crystallization time (s)	180	180	180	10
QD density (cm^{-2})	6×10^8	6×10^8	6×10^8 to 1×10^{10}	2×10^{10}
Ga droplet volume (nm^3)	2.5×10^4	2.5×10^4	V1 = 3.7×10^4 V2 = 1.8×10^4 V3 = 1.8×10^3	C1 = 3×10^2 C2 = 6×10^2 C3 = 1.2×10^3 C4 = 2.4×10^3

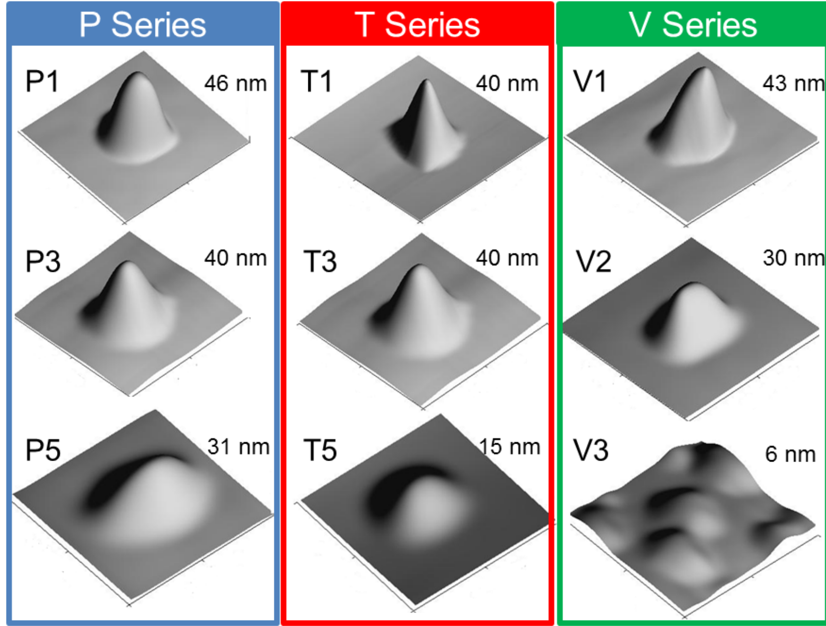

FIG. 1. AFM images (300 nm×300 nm area) of typical QDs grown at different As BEP (P Series - left panel), crystallization temperatures (T Series - central panel) and initial droplet volumes (V Series - right panel). Sample numbers (see Table I) and QD heights are indicated alongside each image.

In all sets, after that 1 ML of Ga was incorporated on the As terminated surface, a RHEED pattern corresponding to the Ga stabilized (4×6) surface reconstruction was observed. The remaining volume of deposited Ga formed liquid Ga droplets. The crystallization, under As flux, of the Ga droplets into QDs was followed in-situ by monitoring the appearance transmission spots in the RHEED pattern.

Typical AFM images of a subset of the DE-QD are shown in Figure 1. A large range of crystallization conditions and droplet volumes (from 10^2 to 10^5 nm^3) are explored. The DE-QDs approximatively have a truncated circular conical shape and s the DE-QD dimensions and aspect ratio exhibit clear dependence on the growth conditions. The DE-QDs show a dependence of the lateral faceting on the initial Ga droplets volume [44] and the crystallization conditions. In particular, the DE-QDs belonging to the P and T series, although originating from identical Ga droplets, show a broad range of aspect ratios, with heights varying from 20 nm to 55 nm and DE-QD diameters ranging from 100 to 200 nm (see Figure 2, where typical AFM profiles of DE-QDs of the two series are reported).

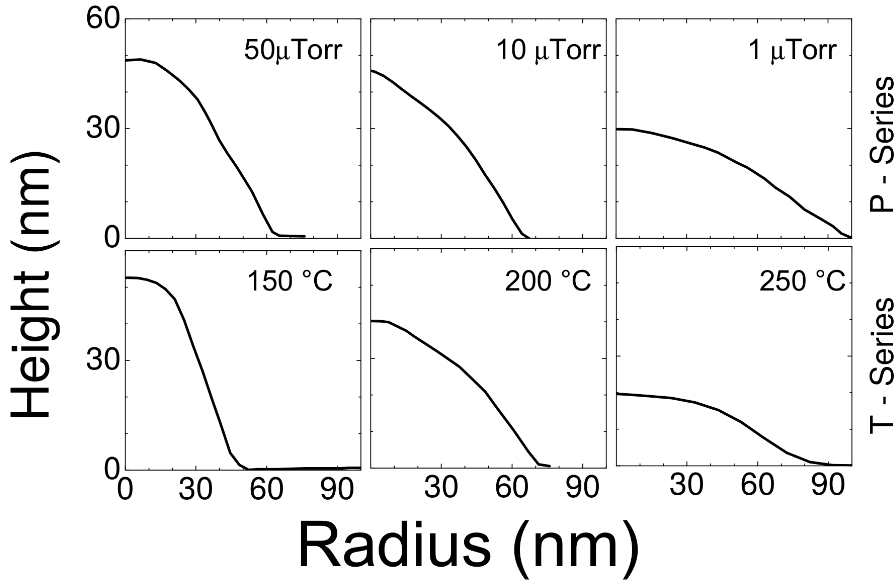

FIG. 2. AFM profiles of typical QDs grown at different As BEP (P Series) and crystallization temperatures (T Series)

At high As flux and low crystallization temperature the DE-QDs show a relatively high aspect ratio ($\rho = 0.6$). As the As flux decreases and/or the crystallization temperature increases, the DE-QD ρ decreases (see Figure 3) and the DE-QDs become slightly elongated along the $[1\bar{1}0]$ direction. None of the DE-QDs have straight facets. In the lower part of the DE-QDs, the exposed facets are steeper and well defined. In the upper part the slope decreases, whereas the top is generally flat. We focused on the DE-QD aspect ratio and faceting. We defined the slope of facets as the tangent of the angle θ between DE-QD surface and substrate. Its dependence on the growth parameters is shown in Figure 3. The facet orientation angle depends strongly on the As flux and on the crystallization temperature. The slope of the facet increases with increasing As flux and decreasing crystallization temperature.

X-STM makes possible the analysis at the atomic scale the shape and the faceting of these DE-QDs after capping. This is of crucial importance as the capping layer has proven to affect strongly the final morphology of the QDs in the case of SK-QDs, where the capping layer can be engineered in order to introduce some degree of control in the SK-QDs height and shape [45]. Topographic images of a typical QD for different volumes of the initial Ga droplet are shown in Fig. 4. All the images were recorded at high negative bias voltages

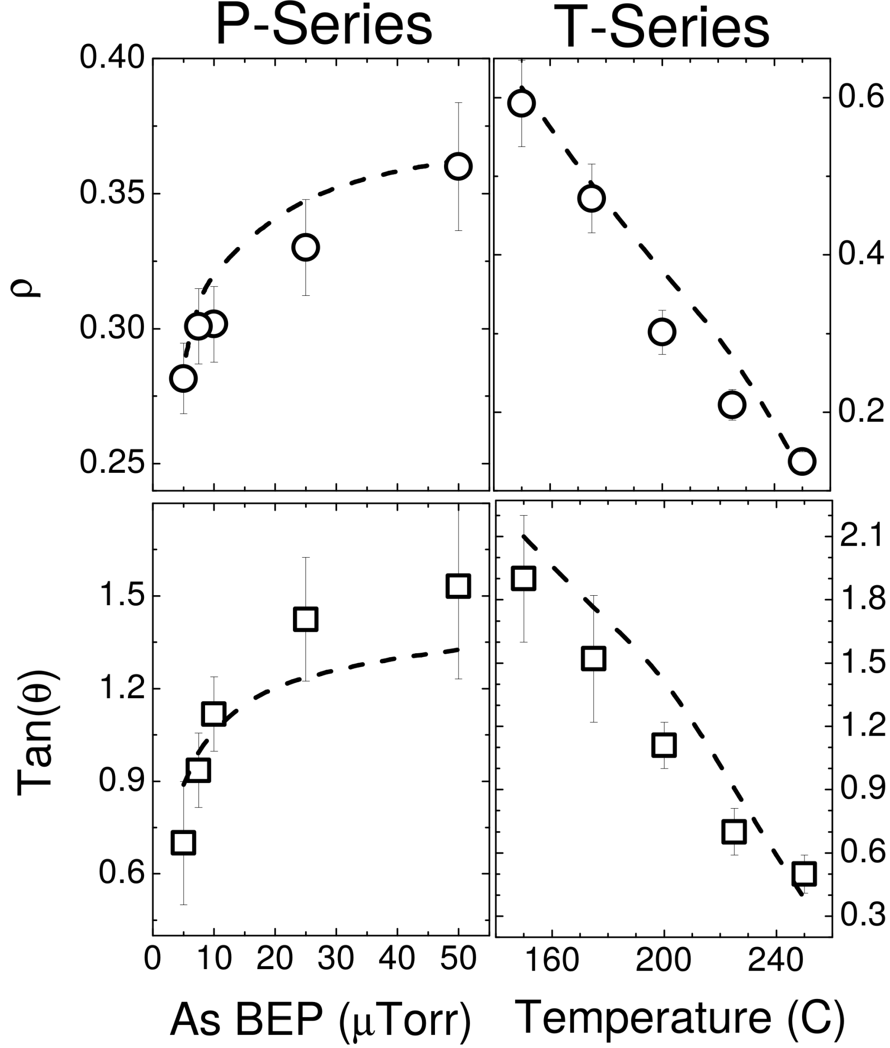

FIG. 3. Dependence, on the crystallization parameters, of the DE-QD aspect ration ρ and facet angle θ. θ is the angle between QD facet and substrate. Upper panels: ρ dependence on As BEP (a) and crystallization temperature (b). Lower panels: θ dependence on As BEP (c) and crystallization temperature (d). The dashed lines indicate the theoretical prediction based on our model.

(-2.5 V). At these tunneling conditions and with the color scaling used, Al atoms give a darker electronic contrast than Ga atoms. Hence, the AlGaAs matrix (ternary compound) appears as an inhomogeneous region while large, bright, homogeneous regions correspond to the GaAs nanostructures (binary compound). Four QD layers grown with different volume of Ga were studied and 167 QDs were analyzed. Overall, the GaAs DE-QDs present fairly sharp interfaces and a low Al intermixing. z-profiles taken across the DE-QDs do not show

any relaxation of the cleaved surface, implying that all these nanostructures are strain-free as expected for lattice-matched AlGaAs/GaAs heterostructures. Also, independently from the volume of Ga used, the wetting layer is maximum 2 ML thick, which is in agreement with Ga deposition on a $c(4 \times 4)$ reconstructed surface [23]. For this analysis, we make the assumption, supported by the AFM data, that the size distribution of the QDs is small. Thus if the QDs are approximatively of equal height, the height distribution for each layer observed by X-STM is due to the random position of the cleavage plane relative to the center of each QD. In this perspective, the highest QDs observed are considered as cut through their center. This way, we can respectively attribute a standard QD height for 1.5 ML, 2 ML, 3 ML and 5 ML of Ga deposited of 12 ML (3.4 nm), 16 ML (4.5 nm), 26 ML (7.3 nm) and 44 ML (12.4 nm). We found that the average QD diameter along the [110] direction increases with the volume of Ga from 35 nm for 1.5 ML Ga to 50 nm for 5 ML. An elongation of the diameters is observed in the $[1\bar{1}0]$ direction with respect to the [110] direction. This elongation originates from the anisotropic diffusion of Ga atoms during the annealing step [46]. The variation in height is much stronger than the variation in diameter with increasing volume of Ga. The change in aspect ratio along the [110] and $[1\bar{1}0]$ directions is illustrated in Figure 5, where the QD aspect ratio is plotted against the volume of Ga deposited. In each direction, the aspect ratio does not depend linearly on the volume of Ga. Because of the arbitrary position of the cleavage, defining the exact shape of the QDs is difficult and has to be done carefully. From the X-STM images, we know that the QDs exhibit a (001) top facet. The absence of triangular shaped cross-sections and the fluctuations of cross-section base diameters within each layer exclude the possibility of truncated pyramidal QDs. This indicates a truncated shape with a circular base instead of a squared base, thus in agreement with AFM measurements. Moreover, as the volume of Ga increases, the aspect ratio dispersion in the cross-sectional STM cuts increases strongly indicating that: (i) small QD proportionally have a wider (001) top facet, (ii) the QD sides are not straight, (iii) the angle θ is not constant.

From AFM and X-STM images (Figures 1, 2 and 4), the approximate DE-QD shape in the whole investigated growth parameter range is a truncated cone, whose major (R_M) and minor (r_m) radius and height (h) depends on the actual Ga droplet crystallization conditions (see inset in Figure 5). From experimental DE-QD profiles we also find a proportionality between the major and minor radius of the DE-QDs: $r_m = \alpha R_M$, being $\alpha = 0.45$.

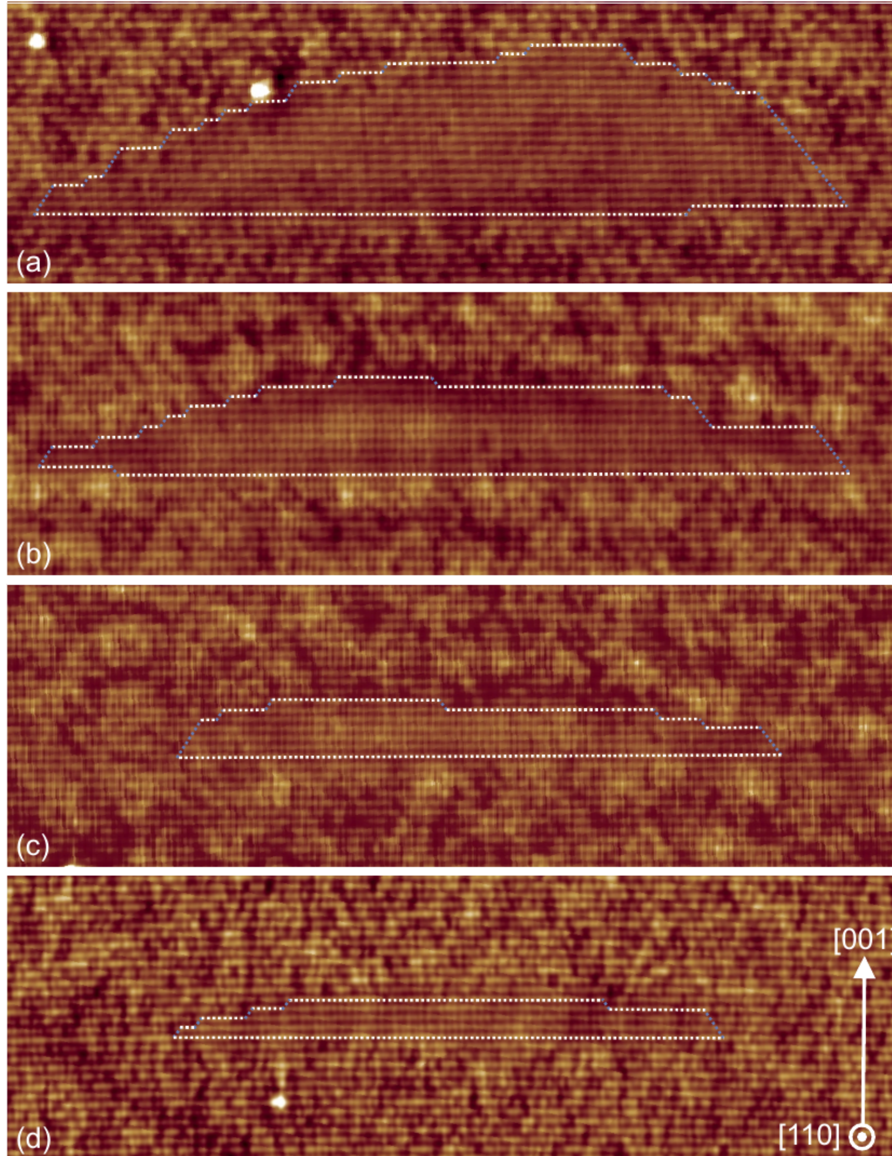

FIG. 4. 53 nm×17 nm filled states topography images of QDs for (a) 5 ML, (b) 3 ML, (c) 2 ML and (d) 1.5 ML of Ga. The images correspond to 2D cuts close to the center of the QDs. (110) facets are outlined in white and (111B) facets are outlined.

The data in the AFM series P, T and V show a continuous transition between surfaces with different orientation angle. This is a peculiar feature of the DE-QDs. To understand the surface structure of QDs which allows for such continuous tuning of surface facet orientation, AFM and X-STM accurate analysis of surfaces and interfaces have been carried out. Ref. 47 reports that the DE-QDs sidewalls are characterized by stepped facets, which present a combination of alternating (001) terraces separated by (111)B facets. The presence of such

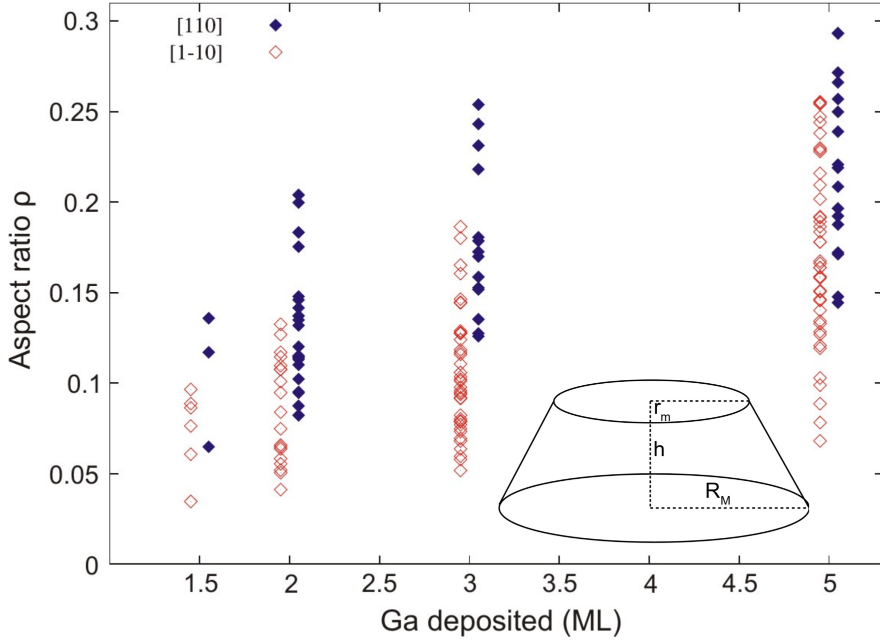

FIG. 5. Aspect ratio as function of the volume of Ga deposited for all the capped QDs analyzed by X-STM along the [110] direction (closed symbols) and [1$\bar{1}$0] direction (open symbols). The aspect ratio does not depend linearly on the volume. The dispersion increases with the volume of Ga indicating that: (i) small QD proportionally have a wider (001) top facet ,(ii) the QD sides are not straight, (iii) the angle θ is not constant. The difference between the [110] and the [1$\bar{1}$0] directions reflects the elongation of the QDs along the [1$\bar{1}$0] direction. Inset: schematic DE-QD shape.

stepped sidewalls can be also traced in our QDs. In Fig. 6 we report the AFM profile and its derivative of a DE-QD belonging to sample V3. Clear plateaus in the QD profile derivative are present, thus indicating a stepped morphology of the QD sidewalls.

The determination of facets orientation of the QD stepped sidewalls can be done in X-STM measurements, which allow for an atomic resultion of the interface morphology. As can be seen in Fig. 4, the DE-QD/barrier interfaces present the expected combination of alternating (001) terraces separated by (111)B facets[47]. The (001) facets are wider for DE-QDs with low ρ and θ (Fig. 4c and 4d), than for those with a larger aspect ratio and facet angle (Fig. 4a and 4b). As a result the number of (111)B facets is much higher for the QDs with an high aspect ratio. Angles θ between 54° and 10° are obtained by an extension of (001) terraces and a reduction of (111)B steps when moving from high to low angle surfaces, allowing the system to expose minimal energy surfaces. Angles above 54°, observed at low

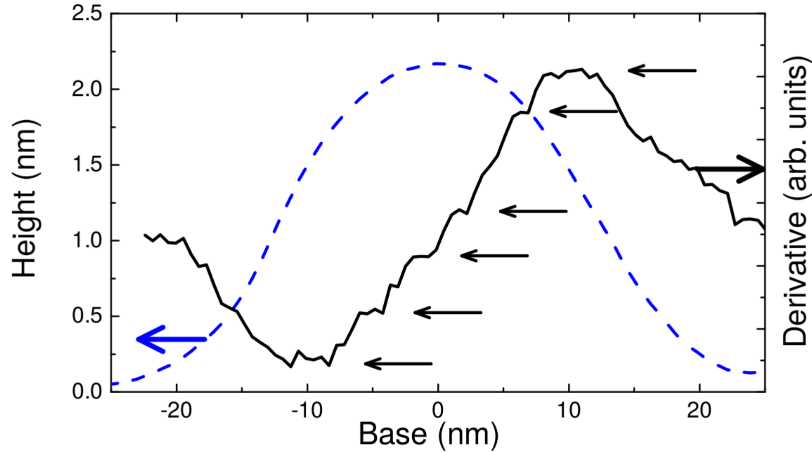

FIG. 6. AFM profile (blue dashed line, left scale) and profile derivative (black line, right scale) of a QD belonging to sample V3. Black arrows indicate the appearence of plateaus on the profile derivative.

T and high As flux, may stem from the additional presence of {100} or {110} steps. The comparison and the good agreement between the AFM and X-STM data reveals the crucial point that the shape of the QDs is not altered upon capping. The dimensions and the exposed facets are preserved after capping.

DISCUSSION

The DE-QD aspect ratio and side facet angle appear to continuously vary in the range 0.05–0.6 and 10°–65°, respectively, by choosing the proper crystallization conditions. This is a peculiar characteristic of DE-QDs. In SK-QD systems, like SiGe/Si and InAs/GaAs, well-defined transitions between aspect ratio and facet configurations are shown as a function of the deposited volume [48–50]. The three-dimensional island formation is in fact favored by the strain relaxation despite the higher surface energy. Surface energetics and strain relaxation play a fundamental role and their ratio determine the overall dot shape [50].

The smooth variation in DE-QDs aspect ratio and side facet angle within wide ranges, depending only on the crystallization conditions, suggests a minor role played by surface energetics, compared to growth kinetics, in DE-QD formation. The DE-QD formation process

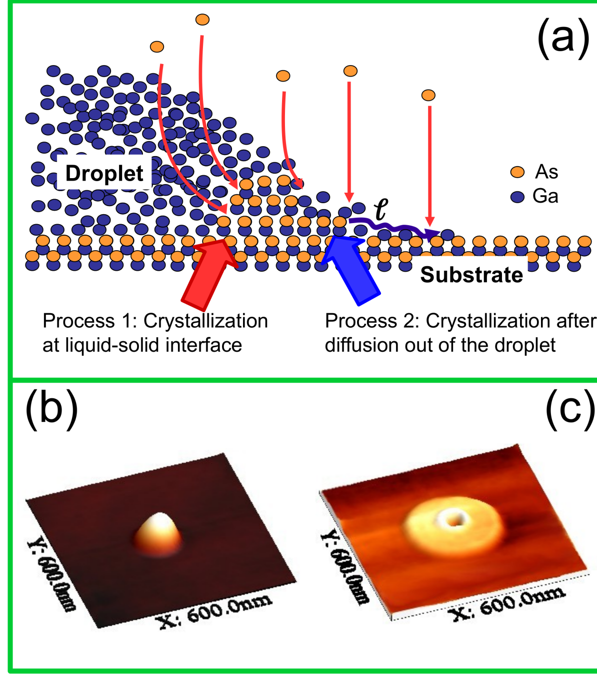

FIG. 7. Panel (a): Schematic explanation of the DE-QD growth mechanism during As supply. Process 1: As direct incorporation in the metallic droplet gives rise to GaAs crystallization at the liquid-solid interface, starting from the triple line. Process 2: Owing to As adsorption on the surface surrounding the droplet, surface termination is changed and diffusion of Ga out of the droplet by capillary forces take place. Coming from the droplets edge, Ga atoms can migrate covering a mean displacement lenght ℓ before being incorporated into the GaS crystal. Blue dots indicate Ga atoms. As atoms are indicated by yellow dots. Panel (b): typical AFM image of a DE-QD obtained As incorporation and Ga crystallization at the liquid-solid interface. Panel (c): DE nanostructure fabricated by Ga diffusion controlled crystallization dynamics.

is strongly influenced by the diffusion of Ga atoms out of the droplet towards thermodynamical equilibrium in presence of an As flux [24, 25, 51], which is, for this system, a two dimensional GaAs layer wetting the AlGaAs substrate.

The GaAs/AlGaAs DE-QD self-assembly thus strictly relies on the crucial and kinetically limited processes of crystallization and Ga diffusion. [23] During the Ga droplet crystallization under As flux, the relative importance of two processes proceeding in parallel determines the final crystal morphology (see Fig 7):[23, 52]

1. the As incorporation in the metallic droplet and the GaAs crystallization at the liquid-

solid interface ;

2. the As adsorption on the surface surrounding the droplet changing the surface termination and providing the thermodynamic driving force for the diffusion of Ga out of the droplet by capillary forces.

The As atoms impinging on the droplet during the crystallization step are dissolved into the liquid Ga. The GaAs crystallization then proceeds within the droplet by nucleation at the triple point (see process 1 in Figure 7) [53]. The crystalline GaAs forms at this stage is a ring at the perimeter of the droplet. The ring increases in thickness during As deposition and eventually merges to form a compact island [53]. At the same time, Ga adatom diffusion and Ga-As bond formation on the surface around the droplet lead to the accumulation of GaAs material within a diffusion length of Ga adatoms from the droplet edge (see process 2 in Fig. 7). Temperature and As pressure govern the relative weight of each process. The GaAs nanocrystal profile is therefore expected to be dependent on the ratio between the crystallization velocity at the liquid-solid interface within the droplet and the radial diffusion, and crystallization at the substrate surface, of Ga from the droplet edge. As a matter of fact, two estreme nanostructure morphologies are expected. In the case dominated by growth at the liquid-solid interface within the droplet, compact island morphologies are expected (Fig. 7b) while on the opposite, when diffusion from the droplet edge controls the Ga crystallization dynamics, hollow morphologies, like disks and rings are expected (Fig. 7b)[23, 52]. In between these two extremes, more complex mophologies, like double ring and molecules, can be obtained. [30, 35, 37, 40]

In view of all these considerations, the main physical parameter governing the regimes for QD formation is the diffusion length of Ga from the droplet edge $\ell = \sqrt{4D_{\mathrm{Ga}}\tau}$, which depends on temperature and As flux through the diffusivity $D_{\mathrm{Ga}} = D_0 \exp(-E_A/kT)$ and the lifetime of the Ga adatoms τ. Here E_A is the activation energy of the diffusion process. The Ga adatom lifetime is $\tau = N_s/J_{\mathrm{As}}$, where N_s is the number of surface sites and J_{As} the atomic As flux [54, 55], as a consequence of being droplet epitaxy an As limited growth mode [23]. From our experimental data, we suggest that the accurate control of the Ga diffusion length, via temperature and As flux allows to finely tune the QD shape and dimensions.

In order to test our idea we performed numerical simulations based on a diffusion model and compared them with the experimental DE-QD profiles. Our hypothesis is that the

geometrical DE-QD profile is proportional to the local concentration profile of Ga diffusing from the droplet. Under this assumption, the Ga concentration profile before crystallization is $P(r) = A(r)/\xi$, where $A(r)$ is the experimental profile of the QD, in each series, crystallized at the lowest temperature or the highest As flux and ξ the proportionality factor. This permits to reduce the effects of the diffusion of Ga from the droplet perimeter (process 2) at minimum and allows us to implicitly take into account, at least to the first order of approximation, the complex crystallization dynamics inside the metallic Ga droplet (process 1) [52, 53]. However, this makes the model outcome clearly dependent on the choice of $A(r)$. For this reason we reduced the degree of arbitrariness by setting $A(r)$ to the more probable QD experimental profile within the ensembles in T1 (for T-Series) and P1 (for P-Series).

The QD radial profile, as a function of ℓ is then given by [56]:

$$C(r, \ell) = \frac{2\xi}{\ell^2} \exp\left(\frac{-r^2}{\ell^2}\right) \int_0^\infty P(r') \exp\left(\frac{-r'^2}{\ell^2}\right) I_0\left(\frac{2rr'}{\ell^2}\right) r'dr'. \tag{1}$$

In our analysis, we disregard the anisotropy of the Ga diffusion [57]. In the definition of ℓ we set $D_0 = 0.7$ cm^{2}s^{-1} and $E_A = 1.15$ eV, thus within the limits recently set for Ga adatom diffusion on As terminated surfaces [55, 58]. In Figure 3 we report the comparison between ρ and θ experimental results and diffusion model for the P and T series. The description of the shape evolution given by the model is in excellent agreement with experimental data.

The actual DE-QD shape is then the outcome of a kinetically controlled, through the Ga diffusion length ℓ, Ga diffusion and crystallization. Raising substrate temperature, or decreasing As BEP, induces an increase of ℓ during the crystallization process. The change in aspect ratio and facet angle, which decrease with increasing ℓ, can be therefore interpreted as the consequence of the increase of the DE-QD diameter due to diffusion of Ga out of the droplet.

On the basis of the demonstrated relevance of Ga diffusion in fixing the actual DE-QD shape, a quantitative and direct insight to the DE-QD morphology evolution with the growth parameters can be gained through a simple, parameter free model, which describes the evolution of the DE-QD morphology as a function of droplet volume and crystallization condition.

As previously stated, the approximate DE-QD shape, in the whole investigated growth parameter range, is a truncated cone (see Fig. 5) with $r_m = \alpha R_M$, where $\alpha = 0.45$. The DE-

QD volume V is related to the initial droplet volume V_0 and radius R_0 via the relation $V = \beta V_0 = \beta\gamma R_0^3$. Assuming that each Ga atom in the droplet contributes to the formation of the DE-QD, because of the low crystallization temperature, β is the ratio $\beta = V_{\mathrm{GaAs}}/V_{\mathrm{Ga}} = 2.31$ between the volume $V_{\mathrm{GaAs}} = 4.52 \times 10^{-29}\,\mathrm{m}^3$ of a GaAs molecule inside the GaAs crystal and the atomistic volume of Ga in the liquid droplet $V_{\mathrm{Ga}} = 1.96 \times 10^{-29}\,\mathrm{m}^3$. The proportionality constant γ is set by the contact angle between the metallic Ga and the substrate. $\gamma = 0.7$ in our experiments.

Under As pressure, the Ga diffusion on the As terminated surface increases the radius of DE-QD base by a diffusion length: $R_M = R_0 + \ell$. Changing the diffusion length ℓ via temperature and As flux, at constant QD volume V, directly affects QD height and facet through the dependence of R_M on ℓ. Increasing the DE-QD radius at constant DE-QD volume therefore reduces the DE-QD height and consequently the DE-QD aspect ratio $\rho = h/2R_M$ and the facet angle $\tan(\theta) = h/(R_M - r_m)$. With simple geometrical considerations, we can express θ and ρ as a function of the ratio of two observable quantities, the droplet (R_0) and the DE-QD (R_M) radius:

$$\tan(\theta) = \frac{3}{\pi}\frac{\beta\gamma}{(1-\alpha^3)}\left(\frac{R_0}{R_M}\right)^3, \tag{2}$$

$$\rho = \frac{3}{2\pi}\frac{\beta\gamma}{(1+\alpha+\alpha^2)}\left(\frac{R_0}{R_M}\right)^3. \tag{3}$$

Equations (2) and (3) are fit parameter free and independent on the actual growth conditions. The agreement between the predicted behavior and the experimental data of both θ and ρ, shown in Fig. 8, is remarkable thus indicating, one more time, the fundamental role played by Ga diffusion, during As induced crystallization in determining the final DE-QD morphology.

It is worth noting that Equations (2) and (3) predict the dependence of ρ and θ on the initial droplet volume, at fixed crystallization conditions, which was observed in sample series V and $\mathrm{V_{cap}}$ and Ref. [44]. Fixing substrate temperature and As BEP during crystallization sets the Ga diffusion length ℓ in the experiments. This makes $R_0/R_M = (1 + \ell/R_0)^{-1}$ an increasing function of the droplet volume V_0. Therefore, our theory predicts the DE-QD aspect ratio and the facet orientation angle to increase with the droplet volume. As a matter of fact, changing the initial droplet volume has only minor effect on R_M as $R_0 \propto V_0^{1/3}$, so the

increase of the final DE-QD volume affects QD height only. Again, no sharp transition on the dependence of ρ and θ on R_0/R_M is observed, as expected for a system driven by energy minimization and not influenced by any minima in the QD morphology energy landscape.

A fundamental outcome of Equations (2) and (3), together with the possibility, given by DE, to determine the QD volume by the initial Ga droplet, is that DE-QD size and aspect ratio can be independently engineered by a suitable choice of the Ga deposition and As crystallization conditions. This is of the utmost importance when a fine tuning of the QD electronic properties is necessary to improve QD based devices, like single photon emitters, detectors or solar cells [10, 13, 16]. Simple electronic quantum confinement considerations, in fact, indicate that the ability to control independently QD size and aspect ratio permits the independent control of QD emission energy and electronic inter–level energy spacing. The latter is extremely relevant in shaping electron–phonon interaction in QDs [59–62], a fundamental property of QD for the improvement of quantum devices at room temperature [63, 64].

Post droplet crystallization annealing procedure performed on sample V_{cap} induces a slight change in the QD morphology related to thermally activated mass transport processes driven by the out-of-equilibrium state of DE-QDs [46, 65]. Overall however, the QD morphology is maintained upon capping. Our growth model is still valid after capping and rapid thermal annealing. Also the X-STM data (V_{cap} series) align along the Equation (2) and (3) lines in Figure 8.

CONCLUSIONS

DE-QD morphology is completely determined by the kinetics of droplet Ga crystallization under As flux. The two relevant quantities which set the actual DE-QD shape are the initial droplet volume and the Ga diffusion length ℓ at the droplet crystallization conditions. This permits to independently control size and aspect ratio of GaAs/AlGaAs DE-QDs over wide ranges. The QD faceting undergoes a continuous transition which depends on the initial droplet radius and the diffusion length at the crystallization conditions only. The facets are constituted by a series of steps made by 001 and 111 facets whose length vary depending on the facet angle. The QD morphology is maintained upon capping. Parameter free, simple analytical relations are introduced [equations (2) and (3)] which make it possible to

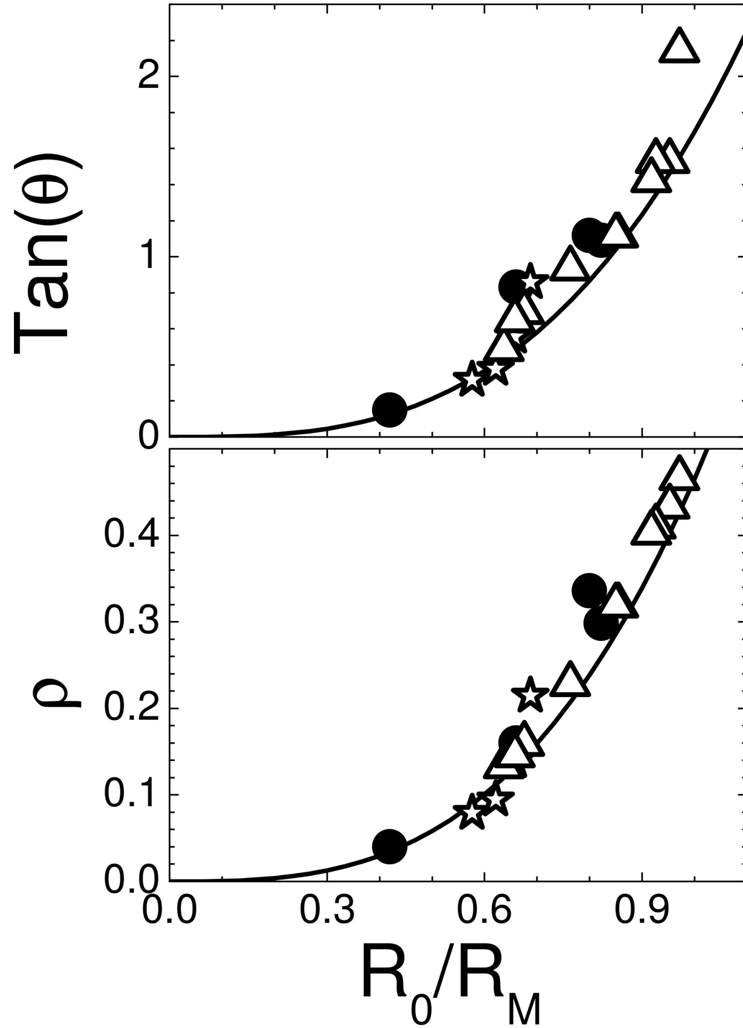

FIG. 8. Left panel: facet angle θ and right panel: aspect ratio ρ as a function of the R_0/R_M ratio for the sets P and T (triangles), V (circles) and the series V_{cap} (stars). The continuous lines are the theoretical prediction obtained using Equations (2) and (3).

make a detailed engineering of the QD electronic properties via growth condition control. Although based on the simple mechanism of controlled diffusion during crystallization, the DE-QD shape engineering mechanism is extremely powerful. It permits the independent achievement of usually incompatible targets, namely QD emission, interband, intervalley, spin-orbit, strain-induced state coupling [4, 5] and electron–phonon scattering [62].

The research was supported by Fondazione Cariplo (COSMOS Project). The authors thank D. Scarpellini for help.

---

* stefano.sanguinetti@unimib.it

[1] M. A. Kastner, Phys. Today **46**, 24 (1993).

[2] D. Bimberg, M. Grundmann, and N. N. Ledentsov, Quantum Dots Heterostructures (Wiley, New York, 1999).

[3] C. Delerue and M. Lannoo, NanostructuresTheory and Modeling (Springer Verlag, Berlin, 2004).

[4] G. Narvaez, G. Bester, and A. Zunger, Phys. Rev. B **72**, 245318 (2005).

[5] J.-W. Luo and A. Zunger, Phys. Rev. B **84**, 235317 (2011).

[6] E. A. Zibik, T. Grange, B. A. Carpenter, N. E. Porter, R. Ferreira, G. Bastard, D. Stehr, S. Winnerl, M. Helm, H. Y. Liu, M. S. Skolnick, and L. R. Wilson, Nat. Mater. **8**, 803 (2009).

[7] A. Tredicucci, Nat. Mater. **8**, 775 (2009).

[8] G. M. Vanacore, J. Hu, W. Liang, S. Bietti, S. Sanguinetti, and A. H. Zewail, Nano Lett. **14**, 6148 (2014).

[9] P. Bhattacharya and Z. Mi, Proc. IEEE **95**, 1723 (2007).

[10] P. Martyniuk and A. Rogalski, Prog. Quantum Electron. **32**, 89 (2008).

[11] G. Scalari, C. Walther, M. Fischer, R. Terazzi, H. Beere, D. Ritchie, and J. Faist, Laser Photonics Rev. **3**, 45 (2009).

[12] T. Akiyama, M. Ekawa, M. Sugawara, K. Kawaguchi, A. Kuramata, H. Ebe, and Y. Arakawa, IEEE Phot. Tech. Lett. **17**, 1614 (2005).

[13] S. Strauf, N. G. Stoltz, M. T. Rakher, L. A. Coldren, P. M. Petroff, and D. Bouwmeester, Nat. Photonics **1**, 704 (2007).

[14] L. Cavigli, S. Bietti, N. Accanto, S. Minari, M. Abbarchi, G. Isella, C. Frigeri, A. Vinattieri, M. Gurioli, and S. Sanguinetti, Appl. Phys. Lett. **100**, 231112 (2012).

[15] A. Luque and A. Marti, Phys. Rev. Lett. **78**, 5014 (1997).

[16] A. Mellor, A. Luque, I. Tobias, and A. Marti, Appl. Phys. Lett. **101**, 133909 (2012).

[17] A. Scaccabarozzi, S. Adorno, S. Bietti, M. Acciarri, and S. Sanguinetti, Phys. status solidi - Rapid Res. Lett. **7**, 173 (2013).

[18] A. D. Yoffe, Adv. Phys. **51**, 799 (2002).

[19] X. Li, Y. Wu, D. Steel, D. Gammon, T. H. Stievater, D. S. Katzer, D. Park, C. Piermarocchi, and L. J. Sham, Science (80-.). **301**, 809 (2003).

[20] C. L. Salter, R. M. Stevenson, I. Farrer, C. a. Nicoll, D. a. Ritchie, and A. J. Shields, Nature **465**, 594 (2010).

[21] S. Kiravittaya, A. Rastelli, and O. G. Schmidt, Reports Prog. Phys. **72**, 046502 (2009).

[22] J. T. Robinson, A. Rastelli, O. Schmidt, and O. D. Dubon, Nanotechnology **20**, 085708 (2009).

[23] S. Sanguinetti and N. Koguchi, in Mol. Beam Ep. From Res. to mass Prod., edited by M. Henini (Elsevier Ltd, 2013) Chap. 4, p. 95.

[24] N. Koguchi and K. Ishige, J. Vac. Sci. Technol. B **11**, 787 (1993).

[25] K. Watanabe, N. Koguchi, and Y. Gotoh, Jpn. J. Appl. Phys. **39**, L79 (2000).

[26] T. Kuroda, S. Sanguinetti, M. Gurioli, K. Watanabe, F. Minami, and N. Koguchi, Phys. Rev. B **66**, 121302(R) (2002).

[27] J. G. Keizer, J. Bocquel, P. M. Koenraad, T. Mano, T. Noda, and K. Sakoda, Appl. Phys. Lett. **96**, 062101 (2010).

[28] B. Liang, A. Lin, N. Pavarelli, C. Reyner, J. Tatebayashi, K. Nunna, J. He, T. J. Ochalski, G. Huyet, and D. L. Huffaker, Nanotechnology **20**, 455604 (2009).

[29] A. Urbanczyk, J. G. Keizer, P. M. Koenraad, and R. Notzel, Appl. Phys. Lett. **102**, 073103 (2013).

[30] T. Mano, T. Kuroda, S. Sanguinetti, T. Ochiai, T. Tateno, J. S. Kim, T. Noda, M. Kawabe, K. Sakoda, G. Kido, and N. Koguchi, Nano Lett. **5**, 425 (2005).

[31] Z. M. Wang, K. Holmes, J. L. Shultz, and G. J. Salamo, Phys. Status Solidi **202**, R85 (2005).

[32] M. Jo, J. G. Keizer, T. Mano, P. M. Koenraad, and K. Sakoda, Appl. Phys. Express **4**, 2 (2011).

[33] J. G. Keizer, M. Jo, T. Mano, T. Noda, K. Sakoda, and P. M. Koenraad, Appl. Phys. Lett. **98** (2011), 10.1063/1.3589965.

[34] M. Hanke, M. Schmidbauer, D. Grigoriev, P. Schafer, R. Kohler, T. H. Metzger, Z. M. Wang, Y. I. Mazur, and G. J. Salamo, Appl. Phys. Lett. **89**, 053116 (2006).

[35] M. Yamagiwa, T. Mano, T. Kuroda, T. Tateno, K. Sakoda, G. Kido, N. Koguchi, and F. Minami, Appl. Phys. Lett. **89**, 113115 (2006).

[36] M. DeJarld, K. Reyes, P. Smereka, and J. M. Millunchick, Appl. Phys. Lett. **102**, 133107 (2013).

[37] C. Somaschini, S. Bietti, N. Koguchi, and S. Sanguinetti, Nano Lett. **9**, 3419 (2009).

[38] C. Somaschini, S. Bietti, N. Koguchi, and S. Sanguinetti, Nanotechnology **22**, 185602 (2011).

[39] C. Somaschini, S. Bietti, S. Sanguinetti, N. Koguchi, and A. Fedorov, Nanotechnology **21**, 125601 (2010).

[40] C. Somaschini, S. Bietti, N. Koguchi, and S. Sanguinetti, Appl. Phys. Lett. **97**, 203109 (2010).

[41] T. Mano, M. Abbarchi, T. Kuroda, C. A. Mastrandrea, A. Vinattieri, S. Sanguinetti, K. Sakoda, and M. Gurioli, Nanotechnology **20**, 395601 (2009).

[42] S. Sanguinetti, K. Watanabe, T. Tateno, M. Gurioli, P. Werner, M. Wakaki, and N. Koguchi, J. Cryst. Growth **253**, 71 (2003).

[43] A. Ohtake, Surf. Sci. Rep. **63**, 295 (2008).

[44] C. Heyn, A. Stemmann, A. Schramm, H. Welsch, W. Hansen, and A. Nemcsics, Appl. Phys. Lett. **90**, 203105 (2007).

[45] J. G. Keizer, M. Bozkurt, J. Bocquel, T. Mano, T. Noda, K. Sakoda, E. C. Clark, M. Bichler, G. Abstreiter, J. J. Finley, W. Lu, T. Rohel, H. Folliot, N. Bertru, and P. M. Koenraad, J. Appl. Phys. **109**, 102413 (2011).

[46] S. Adorno, S. Bietti, and S. Sanguinetti, J. Cryst. Growth **378**, 515 (2013).

[47] A. Nemcsics, L. Tóth, L. Dobos, and A. Stemmann, Microelectron. Reliab. **51**, 927 (2011).

[48] A. Rastelli and H. von Känel, Surf. Sci. **532-535**, 769 (2003).

[49] A. Rastelli, M. Stoffel, J. Tersoff, G. S. Kar, and O. G. Schmidt, Phys. Rev. Lett. **95**, 026103 (2005).

[50] G. Costantini, a. Rastelli, C. Manzano, P. Acosta-Diaz, G. Katsaros, R. Songmuang, O. Schmidt, H. V. Känel, and K. Kern, J. Cryst. Growth **278**, 38 (2005).

[51] C. D. Lee, C. Park, H. J. Lee, S. K. Noh, K. S. Lee, and S. J. Park, Appl. Phys. Lett. **73**, 2615 (1998).

[52] K. Reyes, P. Smereka, D. Nothern, J. M. Millunchick, S. Bietti, C. Somaschini, S. Sanguinetti, and C. Frigeri, Phys. Rev. B **87**, 165406 (2013).

[53] S. Bietti, C. Somaschini, and S. Sanguinetti, Nanotechnology **24**, 205603 (2013).

[54] H. Neave, P. J. Dobson, B. A. Joyce, and J. Zhang, Appl. Phys. Lett. **47**, 100 (1985).

[55] S. Bietti, C. Somaschini, L. Esposito, A. Fedorov, and S. Sanguinetti, J. Appl. Phys. **116**, 114311 (2014).

[56] J. Crank, The Mathematics of Diffusion (Clarendon Press, Oxford, 1955).

[57] K. Ohta, T. Kojima, and T. Nakagawa, J. Cryst. Growth **95**, 71 (1989).

[58] V. P. Labella, D. W. Bullock, Z. Ding, C. Emery, W. G. Harter, and P. M. Thibado, J. Vac. Sci. Technol. A **18**, 1526 (2000).

[59] P. Gartner, J. Seebeck, and F. Jahnke, Phys. Rev. B **73**, 115307 (2006).

[60] S. Sanguinetti, M. Guzzi, E. Grilli, M. Gurioli, L. Seravalli, P. Frigeri, S. Franchi, M. Capizzi, S. Mazzuccato, and A. Polimeni, Phys. Rev. B **78**, 085313 (2008).

[61] K. Schuh, P. Gartner, and F. Jahnke, Phys. Rev. B **87**, 035301 (2013).

[62] A. Steinhoff, H. Kurtze, P. Gartner, M. Florian, D. Reuter, A. D. Wieck, M. Bayer, and F. Jahnke, Phys. Rev. B **88**, 205309 (2013).

[63] M. R. Dachner, E. Malic, M. Richter, A. Carmele, J. Kabuss, A. Wilms, J. E. Kim, G. Hartmann, J. Wolters, U. Bandelow, and A. Knorr, Phys. Status Solidi Basic Res. **247**, 809 (2010).

[64] P. Kaer, N. Gregersen, and J. Mork, New J. Phys. **15** (2013), 10.1088/1367-2630/15/3/035027.

[65] M. Jo, T. Mano, and K. Sakoda, Appl. Phys. Express **3**, 045502 (2010).